ACS OMEGA

Open Access

http://pubs.acs.org/journal/acsodf

Article

New Insights into the All-Dry Synthesis of NMC622 Cathodes Using a Single-Phase Rock Salt Oxide Precursor

Mohammad H. Tahmasebi and Mark N. Obrovac*

Cite This: *ACS Omega* 2024, 9, 1916−1924

Read Online

ACCESS | Metrics & More | Article Recommendations | Supporting Information

ABSTRACT: In this study, new insights into the all-dry synthesis of the $LiNi_{0.6}Mn_{0.2}Co_{0.2}O_2$ (NMC622) cathode using a single-phase rock-salt (RS) oxide precursor are provided. It was found that use of a larger amount of excess Li content not only can enhance the electrochemical performance of NMC made from the RS-precursor but also increase the degree of homogeneity of the NMC cathode material. *In situ* XRD analysis showed that lithiation of the RS-precursor (*i.e.*, formation of the O3-phase) starts at a higher synthesis temperature (~450 °C) than that is required when using a hydroxide precursor (HP) and lithium carbonate (~350 °C). Consequently, Li_2CO_3 was consumed by the reaction with the HP at low temperatures before the temperature reached the Li_2CO_3 melting point. In contrast, the reduced lithiation kinetics of the RS-precursor results in the presence of liquid Li_2CO_3 during the synthesis, which rapidly increases the rates of precursor lithiation and increases the NMC primary particle size.

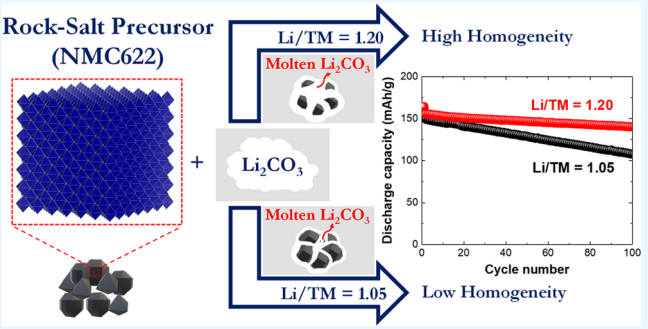

1. INTRODUCTION

Cathode materials for lithium-ion batteries (LIBs) represent a large proportion of their total cost. Much of this cost is associated with the cathode manufacturing process. Currently, layered $LiNi_xMn_yCo_zO_2$ (NMC) cathode materials are the most widely used.[1−9] Several NMC synthesis techniques have been developed, including all-dry,[10,11] hydrothermal,[12] and coprecipitation[13−15] methods. Among these synthesis routes, coprecipitation is used on a large scale and is known for making homogeneous precursors with uniform particle size distributions. Nevertheless, coprecipitation is comparatively complex, involving many process steps, and hence, leading to high energy and water consumption and ultimately high production cost.[10] The molten-salt synthesis process has also been reported as a cost-effective sintering technique in producing homogeneous (both chemical composition and size) single-crystal NMC cathode materials for LIBs. This synthesis technique typically utilizes hydroxide precursors (HPs), and the molten salt is used to enhance crystal growth at lower temperatures. In fact, molten salt techniques require additional steps including washing the products with water which leads to a higher water consumption.[16−22] Accordingly, all-dry NMC synthesis techniques have drawn interest recently in order to reduce cathode synthesis cost and reduce waste substantially.[10,11,23−25]

In our recent studies, we showed that NMC cathodes can be synthesized with an all-dry method using crystalline rock-salt (RS) oxide precursors.[24,26] It was also shown that the compositional homogeneity of the synthesized RS-precursors at the micron-scale (*i.e.*, its compositional microhomogeneity) was directly translated into the compositional homogeneity in the final NMC, which can affect its electrochemical performance.[26] In the present work, new insights into the lithiation mechanism during all-dry synthesis of the NMC622 cathode using the RS-precursor or HP and lithium carbonate are obtained. In addition, the effects of synthesis conditions and excess Li content on microstructural parameters, degree of homogeneity, and electrochemical performance of the NMC cathode made from RS-precursors are further investigated.

2. RESULTS AND DISCUSSION

Figure 1a (bottom panel) shows an XRD pattern of a mixture of NiO, MnO, and CoO powders in a 6:2:2 molar ratio after 3 h grinding. This XRD pattern is characteristic of a mixture of NiO, MnO, and CoO phases with no other impurity phases present which confirms that no chemical reaction occurred between the NiO, MnO, and CoO powders upon grinding. Figure 1a (top panel) shows an XRD pattern of the RS-precursor prepared after heating the ground NiO, MnO, and CoO powder sample at 1000 °C for 12 h under an Ar flow. After this heating process, the initially multiphase mixture is converted into phase-pure RS with a lattice parameter of

Received: November 2, 2023
Revised: November 30, 2023
Accepted: December 6, 2023
Published: December 18, 2023

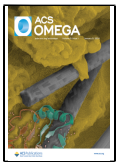

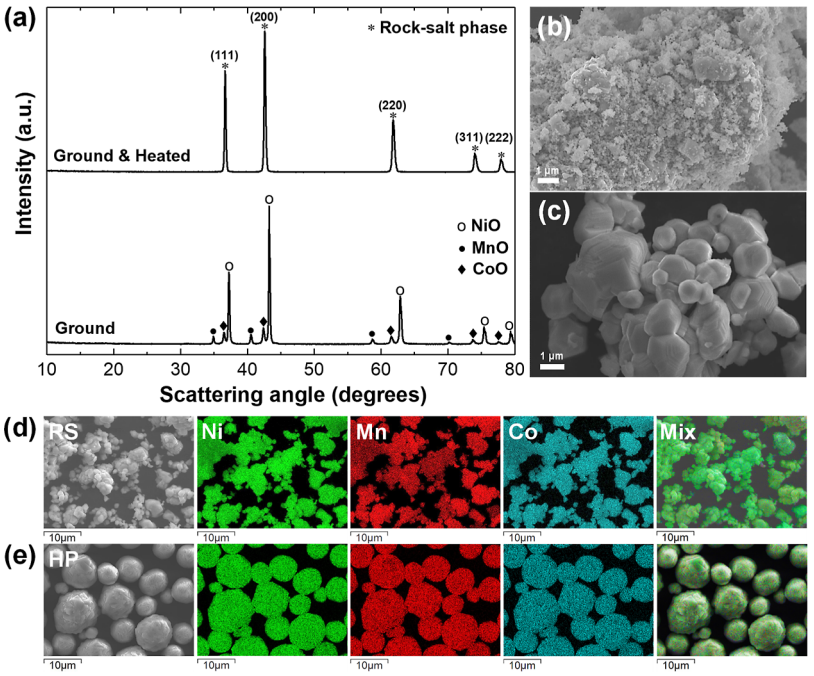

Figure 1. (a) XRD patterns of NiO, MnO, and CoO powders mixture after 3 h grinding and after heating to form RS-precursors. SEM images of the NiO, MnO, and CoO powder mixture after (b) 3 h grinding and (c) after heating to form RS-precursor. SEM images and associated EDX mappings of Ni, Mn, and Co for (d) RS-precursor and (e) HP-precursor.

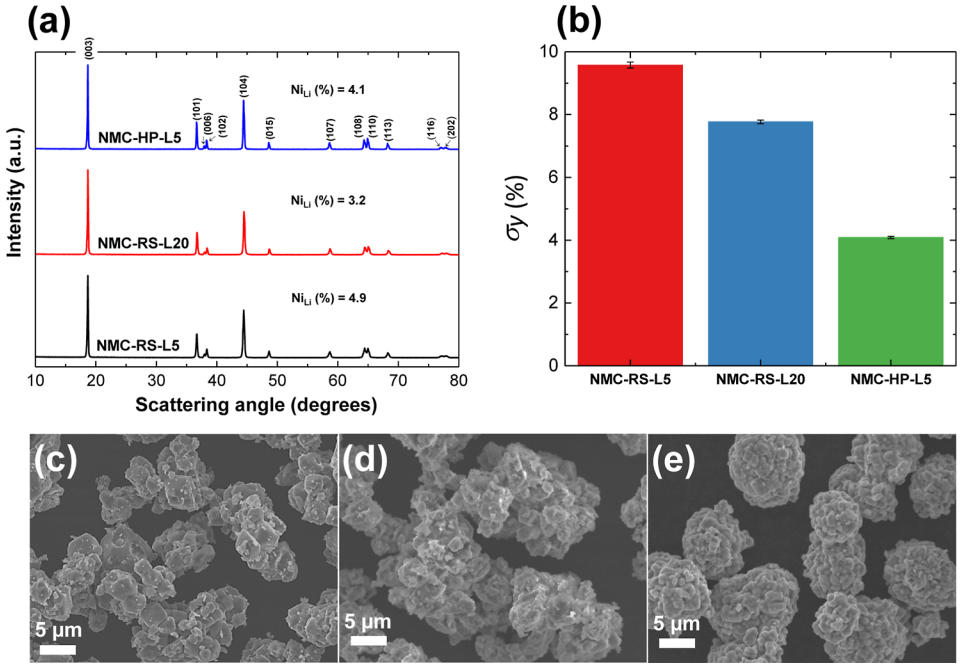

Figure 2. (a) XRD patterns of the NMC622 cathode materials made from RS-precursors with different amounts of excess Li (5 and 20%) and NMC622 made with 5% excess Li from HP-precursor. (b) Standard deviations in Mn distribution (σ_y) for NMCs made from RS and HP-precursors, as determined by the Williamson−Hall method.[26] SEM images of NMC622 cathode materials made from the RS-precursor with (c) 5 and (d) 20% excess Li content; and of (e) NMC622 made with 5% excess Li from the HP-precursor.

4.2413 ± 0.0001 Å, as determined by Rietveld refinement analysis. This is in good agreement with a 6:2:2 linear combination of the lattice constants of NiO, CoO, and MnO, according to Vegard's law (4.2473 Å).

Figure 1b,c shows SEM images for the NiO, MnO, and CoO powder mixture after 3 h grinding and the synthesized RS-precursor, respectively. SEM images of these samples taken at lower magnification are also shown in Figure S4a,b. As shown in Figure 1b, the ground sample consists of small primary particles (0.1−1 μm) that are lightly agglomerated (Figure S4a) into larger (5−20 μm) secondary particles. In contrast, completely different particle morphology was observed for the synthesized RS-precursor where it is composed of faceted primary crystallites (~1−5 μm in size) that are aggregated into

https://doi.org/10.1021/acsomega.3c08702
ACS Omega 2024, 9, 1916−1924

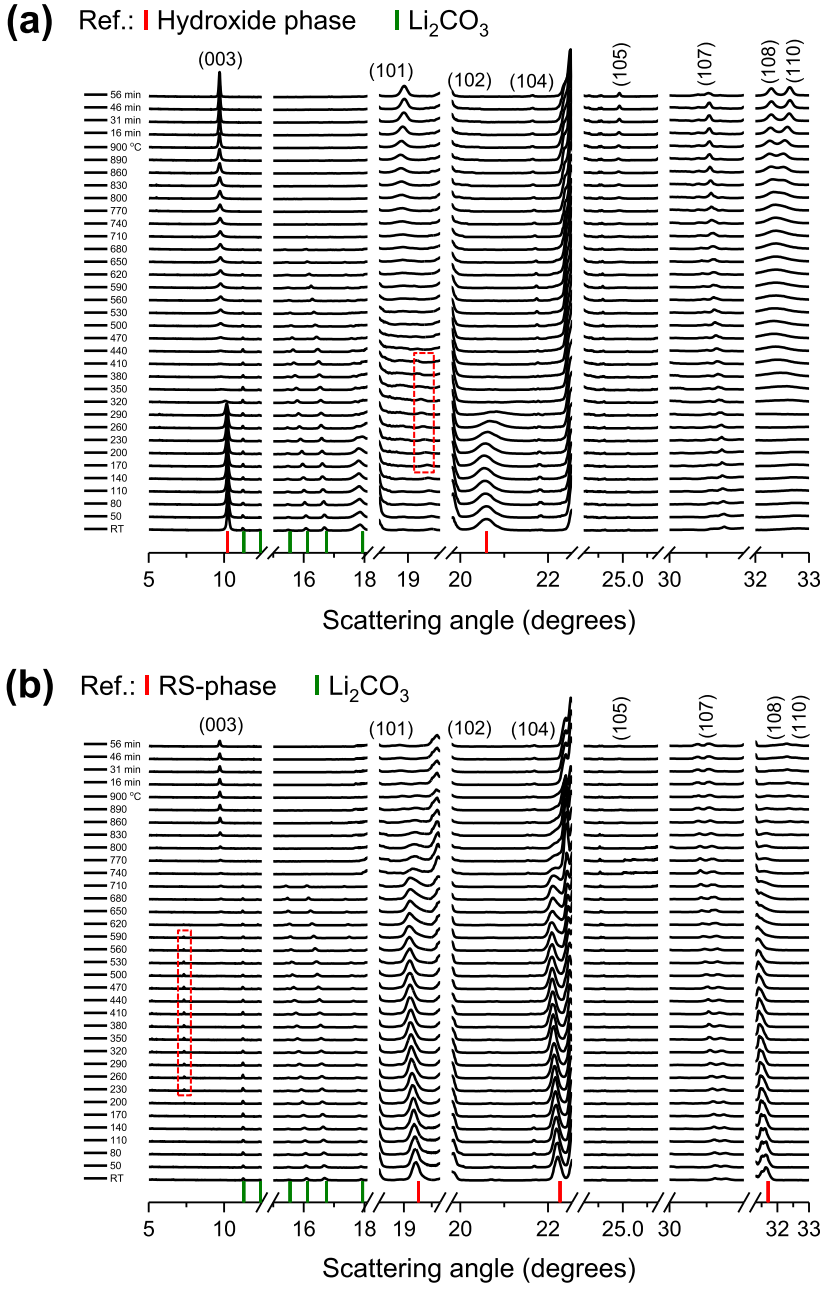

Figure 3. XRD patterns recorded at every 30 °C, from room temperature (RT) to 900 °C and then every 15 min at 900 °C for 1 h, during heating (under an air flow) the mixture of (a) HP-precursor and Li_2CO_3 (NMC-HP-L5) and (b) RS-precursor and Li_2CO_3 (NMC-RS-L5) with a Li/TM ratio of 1.05.

~10−20 μm secondary particles, as depicted in Figures 1c and S4b.

EDS elemental maps acquired for the RS-precursor and a commercial HP are shown in Figure 1d,e. Notably, Ni and Co are uniformly distributed throughout the RS and HP precursors. According to our previous study, the synthesized RS-precursor made by 3 h grinding and heating in Ar showed the lowest degree of Mn-inhomogeneity (σ_x = 1.87 ± 0.02%) compared to other RS-precursors prepared by different grinding times prior to heating.[26] However, a slight inhomogeneity in distribution of Mn (*i.e.*, Mn-depleted regions) is still seen in the RS-precursor (Figure 1d), while Figure 1e reveals a highly homogeneous distribution of Mn in the commercial HP.

XRD patterns of synthesized NMC-RS-L5, NMC-RS-L20, and NMC-HP-L5 cathode materials are presented in Figure 2a. All of the XRD patterns are characteristics of NMC with an O3-type α-$NaFeO_2$ structure with no impurities observed.

Rietveld refinement analysis of the XRD patterns (see further details in Table S1) showed a 4.1% extent of Li−Ni cation mixing for NMC-HP-L5. In contrast, a higher percentage of cation mixing was observed for NMC-RS-L5 (4.9%). This is indicative of the faster lithiation kinetics of the HP compared to the RS-precursor, which we have observed in previous studies.[24,26] The slow lithiation kinetics of the RS-precursor lead to lithium loss due to evaporation during synthesis. The resulting lower amount of lithium available during sintering then leads to cation mixing, as has been shown in previous studies.[24,27,28] For the HP-precursor, lithiation

https://doi.org/10.1021/acsomega.3c08702
ACS Omega 2024, 9, 1916−1924

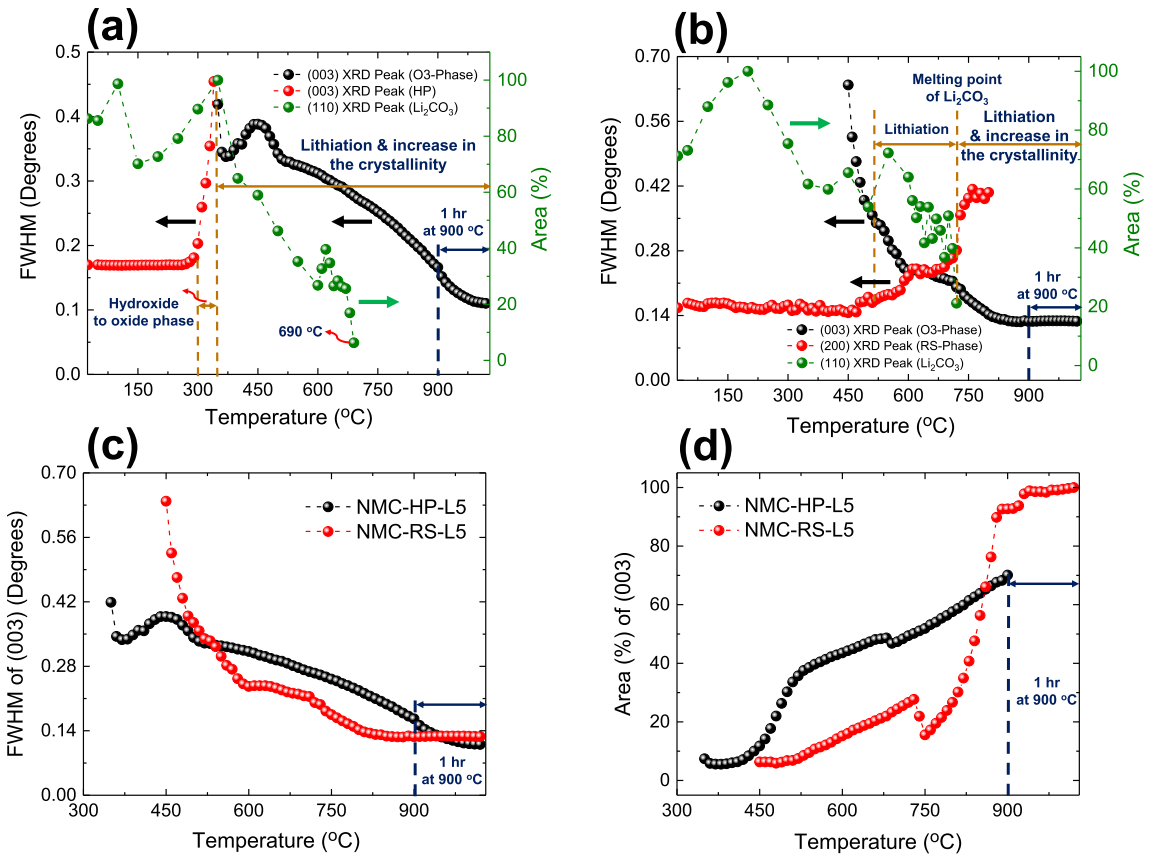

Figure 4. (a) fwhm of the (003) peaks of the O3-phase (NMC phase) and of the hydroxide precursor; and the integrated area of the (110) peak (right axis) of Li_2CO_3 *vs* temperature during the lithiation of HP-precursor. (b) fwhm of the (003) peak of the O3-phase (NMC phase) and the (200) peak of the RS-precursor; and the integrated area of the (110) peak (right axis) *vs* temperature (NMC-RS-L5). (c) fwhm and (d) the integrated (003) peak area *vs* temperature for NMC-RS-L5 and NMC-HP-L5 obtained from the *in situ* XRD analysis. The integrated area under the XRD peaks were normalized to their maximum value.

occurs more quickly, leading to less evaporative lithium loss and more lithium available for thermal lithiation, resulting in a lower cation mixing level. To overcome this issue, a larger excess of lithium was used for the synthesis of NMC from the RS-precursor. As a result, a lower cation mixing extent was obtained for NMC-RS-L20 (3.2%), which is even lower than that obtained for NMC-HP-L5. These results confirm that the all-dry synthesis conditions can significantly affect the final NMC structure.

The degree of inhomogeneity (standard deviation in Mn distribution) in the synthesized NMC cathode materials was also calculated using the XRD data and the modified W−H analysis reported in ref 26. As shown in Figure 2b and Table S1, the degree of compositional inhomogeneity is highest for the NMCs made from the RS-precursors (σ_y = 7.77−9.58%) compared to NMC made from the HP (σ_y = 4.09%). This has been observed previously and is due to the greater level of transition metal mixing in the HP compared to the RS-precursors.[26] Here, it is also observed that significantly less compositional inhomogeneity is present for NMC-RS-L20 (σ_y = 7.77%) compared to that for NMC-RS-L5 (σ_y = 9.58%). This shows that the amount of excess Li_2CO_3 used in the thermal lithiation process during all-dry synthesis effects the transition metal homogeneity of the final NMC. This can occur if Li_2CO_3 is acting as a flux to allow some transition-metal dissolution and transport during the thermal lithiation process. This is likely considering that the melting point of Li_2CO_3 is ∼720 °C, and therefore any unreacted Li_2CO_3 will be in a molten state during thermal lithiation. The presence of Li_2CO_3(l) is confirmed in the analysis of the *in situ* XRD studies below. Therefore, the higher homogeneity in the Mn distribution of NMC-RS-L20 can then be attributed to the larger amount of excess Li_2CO_3 throughout the thermal lithiation step.

Figure 2c−e shows SEM images of NMC622 samples synthesized from the RS and HP-precursors. Overall, as revealed in Figure 2c and d, the NMCs made from RS-precursors consist of primary particles that are ∼1−3 μm in size and aggregated into larger secondary particles (5−20 μm). In contrast, much smaller primary particles (∼1 μm) can be observed for the NMC cathode made from the HP-precursor (Figure 2e). Here, primary particles are distinguished by having clear faceted surfaces. The larger primary particle size of the NMC made from the RS-precursor may be a consequence of the influence of a Li_2CO_3(l) flux that, as will be shown by *in situ* XRD studies below, is present during its thermal lithiation. In contrast, the HP-precursor reacts quickly with Li_2CO_3(s), resulting in no Li_2CO_3 being present above its melting point and leading to less primary particle growth. It needs to be stated that large primary particle growth does not necessarily mean increased crystallinity (*i.e.*, an increased grain size and a reduction in defects). Therefore, while NMC made from HP-precursor has smaller primary particles as observed by SEM, its XRD peaks are narrower, indicating greater compositional homogeneity (as observed by EDS), larger grain size, and possibly less crystal defects.

https://doi.org/10.1021/acsomega.3c08702
ACS Omega 2024, 9, 1916−1924

To understand how the HP- and RS-precursors transform to NMC during the thermal lithiation step, *in situ* XRD analysis was used. Figure 3a,b shows XRD patterns obtained *in situ* every 30 °C from room temperature to 900 °C and every 15 min at 900 °C during heating the HP and RS-precursors with Li_2CO_3 (5% excess Li), respectively. To help follow the structural changes that occur during heating, the changes in the full-width at half-maximum (fwhm) and peak areas of selected peaks are shown in Figure 4.

In terms of the synthesis of NMC from HP and Li_2CO_3 (NMC-HP-L5), peaks from HP and Li_2CO_3 are both apparent in the XRD pattern measured at room temperature. As the temperature is increased, the HP peaks start to decrease in intensity and then completely disappear above ∼300 °C. Simultaneously, peaks from a new phase are consistent with a transition-metal oxide rock salt phase form (highlighted by the red box in the XRD patterns). This is consistent with a previous study by Weber *et al.*,[29] where it was reported that conversion of $Ni(OH)_2$ to oxide phase occurs at ∼267 °C. The peaks from the transition-metal oxide rock salt phase are broad, indicating small crystallites and/or poor crystallinity. An increase in the fwhm of the (003) peak for the hydroxide phase at ∼300 °C (Figure 4a) also confirms the transformation of the hydroxide to an oxide RS phase. This phase is short-lived as it is consumed by the reaction with Li_2CO_3 to form a layered NMC phase, as evidenced by the appearance of an NMC(003) peak at above ∼350 °C, which is coincident with a reduction in the intensity of Li_2CO_3 peaks. This occurs simultaneously with a remarkable increase in the fwhm of the HP (003) peak, where the HP peaks completely disappear. Similar trends can be seen for the integrated areas under (003) XRD peaks for the NMC phase and HP, as shown in Figure S5a. As the temperature is increased, the integrated area under the Li_2CO_3(110) peak continuously decreases up to ∼690 °C where Li_2CO_3 peaks completely disappear (Figure 4a). This is below the melting point of Li_2CO_3 (723 °C), indicating a fast reaction of Li_2CO_3 with the HP in the solid phase. This explains the reduced crystallinity observed for the NMC made by HP since no liquid Li_2CO_3 is present during the synthesis to aid in NMC crystallization. The fwhm of (003) for the NMC phase continuously decreases, indicating an increase in the degree of crystallinity, with further increasing temperature. An expanded view of the (003) XRD peak during heating HP and Li_2CO_3 is provided in Figure S6a. As can be seen, after reaching 900 °C, the only peaks present are of the NMC phase, which continue to sharpen as the temperature is held at 900 °C, indicating further increased crystallinity. Therefore, the crystallization of NMC from the HP-precursor is slow and continues over an extended period of time, even continuing for nearly 1 h after the temperature has reached 900 °C.

XRD patterns measured during the synthesis of NMC from the RS-precursor and Li_2CO_3 (NMC-RS-L5) are shown in Figure 3b. The fwhm of the (003) NMC phase and (200) RS-phase XRD peaks and the integrated area under the (110) lithium carbonate peak as a function of temperature are shown in Figure 4b. Peaks from the RS-precursor and Li_2CO_3 are both apparent in the XRD pattern measured at room temperature. As the temperature is increased, a new phase is formed at ∼200 °C with a large superstructure, as indicated by the XRD peak at ∼7.4°, corresponding to a *d*-spacing of ∼12 Å; however, the RS-precursor peaks remain. Figure S6b shows a detailed view of the XRD peak associated with this new phase in the temperature range of 230−590 °C. As it can be seen, the new phase remains stable up to ∼600 °C and then disappears. We have tried to isolate this phase by heating RS-precursor and Li_2CO_3 mixtures of the same composition in air at temperatures between 200 and 600 °C and then quenching but were not successful. If this new phase exists, it appears not to be stable at room temperature. A possible explanation for this new phase is that the RS-precursor lithiates according to a staging mechanism, which would result in the formation of superstructure peaks, while the RS-phase peaks would remain.

As the reaction temperature between the RS-precursor and Li_2CO_3 is increased, the integrated areas under the RS-phase (200) peak and the Li_2CO_3(110) peak simultaneously decrease up to ∼710 °C (Figure S5b) where the XRD peaks of lithium carbonate disappear due to the melting of Li_2CO_3 at ∼720 °C, as revealed in Figure 3b. This is also consistent with the changes in the integrated area under of Li_2CO_3(110) peak *vs* temperature, as shown in Figure 4b. Interestingly, the start of the formation of the layered structure (O3-phase) occurs above ∼450 °C, which is a higher temperature than the level of formation of the O3-phase from the HP-precursor (350 °C), suggesting sluggish lithiation kinetics. As shown in Figure 4b, as the NMC O3-phase begins to form, the fwhm of the NMC(003) peak begins to decrease, indicating the formation of NMC crystallites with an increasing degree of crystallinity (*i.e.*, reduced defects/increased grain size), while simultaneously the fwhm of RS-phase (200) peak starts to increase, suggesting grain size reduction or the introduction of defects as this phase is consumed. Unlike the HP-precursor, the fwhm of the NMC(003) peak does not decrease continuously. Instead, lithiation of the RS-precursor starts at ∼450 °C. During this period in the reaction, the NMC(003) peak gains in intensity, while the Li_2CO_3(110) peak reduces, indicating the formation of NMC and the consumption of Li_2CO_3. At the same time, the NMC(003) peak fwhm becomes lower (Figure 4b), indicating an increase in the degree of crystallinity. At about 600 °C, the rate at which the fwhm becomes narrowed is reduced, while the intensity of the NMC(003) peak continues to grow, indicating that nucleation may be outpacing NMC crystallization. At 720 °C, the Li_2CO_3 peaks disappear as this phase melts. At the same time, there is a discontinuity in the NMC(003) peak intensity, from the sample shifting in the sample tube, due to the melting of Li_2CO_3. After the discontinuity, a rapid decrease in the NMC(003) peak fwhm and a rapid increase in the NMC(003) peak intensity follow, indicating further improvement of the NMC crystallinity and rapid RS-phase lithiation facilitated by a Li_2CO_3(l) flux. Both the lithiation reaction and crystal growth are complete by 800 °C.

The nature of the lithiation reaction of the RS-precursor is significantly different from the lithiation reaction of the HP-precursor. These differences can be clearly seen in Figure 4c,d, which directly compare the evolution of the NMC(003) fwhm and integrated area. As shown in Figure 4c, the NMC(003) peak forms at a lower temperature for the HP-precursor, followed by continual NMC crystallization. In contrast, NMC forms at a higher temperature from the RS-precursor, and NMC crystallization occurs in stages, with rapid crystallization occurring at the melting point of Li_2CO_3. This rapid crystallization leads to the NMC crystallization process being complete earlier than that for NMC made from the HP-precursor, which did not benefit from the presence of a liquid Li_2CO_3 flux. However, the fwhm of the NMC(003) peak reached the same values for NMC-HP-L5 and NMC-RS-L5

https://doi.org/10.1021/acsomega.3c08702
ACS Omega 2024, 9, 1916−1924

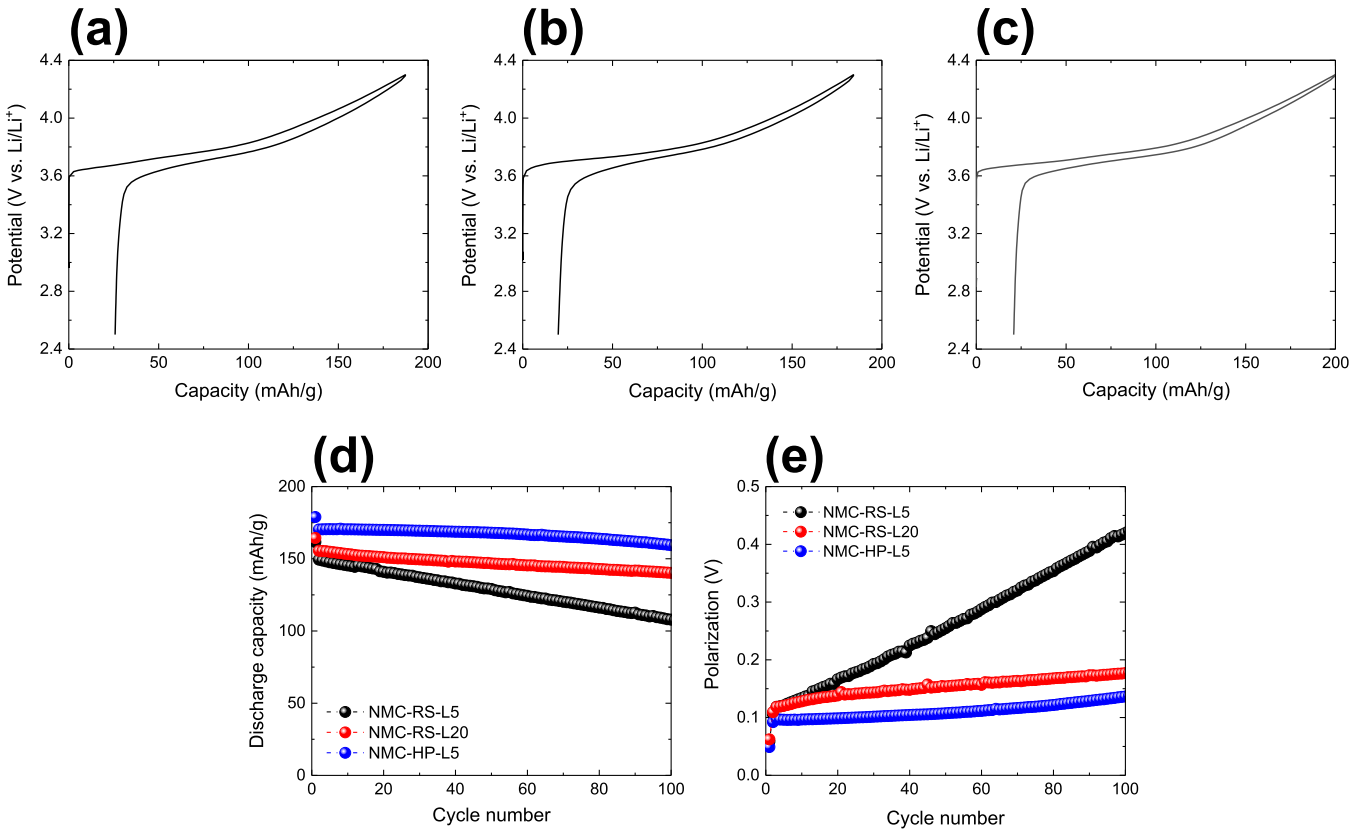

Figure 5. First cycle potential *versus* capacity profiles for (a) NMC-RS-L5, (b) NMC-RS-L20, and (c) NMC-HP-L5. (d) Cycling performance and (e) polarization changes over cycling for NMC-RS-L5, NMC-RS-L20, and NMC-HP-L5.

samples after holding for 1 h at 900 °C, which means that a similar degree of crystallinity was achieved for both NMCs (see also Figure S6a,c). However, because of the presence of the Li_2CO_3(l) flux, the primary particle size, as observed by SEM, is much larger for the NMC made from the RS-precursor than that for the HP-precursor.

The evolution of the NMC(003) peak integrated areas shown in Figure 4d also shows significant differences between the NMC made from HP and RS-precursors. The NMC(003) peak forms earlier for the NMC made from HP-precursor and grows in area quickly and at a much lower temperature (~450 °C) than that for NMC made from the RS-precursor. These *in situ* XRD results confirm the sluggish kinetics of the reaction between Li_2CO_3(s) and RS-precursor compared to that with HP, as reported in our recent study.[24] Unlike what was observed for the HP, the sluggish thermal lithiation kinetics of the RS-precursor results in the presence of the RS-phase up to ~800 °C and the presence of Li_2CO_3(s) up to its melting point (Figure 4b). This is followed by rapid lithiation, facilitated by a Li_2CO_3(l) flux, such that the degree of lithiation overtakes that of the NMC made from the HP-precursor at about 780 °C. By continual heating, both NMCs complete the lithiation process. These results show that NMC made from both HP- and RS-precursors gain the same level of crystallinity and reach full lithiation (as long as sufficient Li_2CO_3 is present), which is confirmed by the Rietveld refinement results. The major difference between these NMCs is a lower degree of compositional homogeneity and a larger primary particle size for the RS-precursor.

Figure 5a–c shows the first cycle voltage curves of NMC-RS-L5, NMC-RS-L20, and NMC-HP-L5, respectively. Figure 5d,e shows the discharge specific capacity and cell polarization, respectively, over 100 charge–discharge cycles for these NMCs. The first reversible capacities (RCs), first irreversible capacities (ICs), initial Coulombic efficiencies (ICEs), and capacity retention over 100 cycles (relative to the specific capacity at the second cycle) of these cells are listed in Table S2. The NMC-RS-L5 sample had the lowest RC (161.6 mA h/g), lowest ICE (86.2%), and the highest polarization, which increased steadily during cycling, resulting in a linear capacity fade. This is due to its high degree of cation mixing, lithium deficiency, and compositional inhomogeneity in this sample. In contrast, NMC-RS-L20 had a higher initial RC (164.4 mA h/g) and ICE (89.3%). The polarization for this sample remained low, resulting in low capacity fade.

The NMC-HP-L5 sample had the highest RC (178.9 mA h/g), ICE (89.6%), and lowest polarization. The higher compositional inhomogeneity and larger primary particle size of the NMC-RS-L20 sample may have contributed to its lower capacity and slightly higher polarization compared to NMC-HP-L5. In a future publication, we will show how the compositional homogeneity of the all-dry synthesis of NMC from RS-precursors can be further improved, leading to the improved electrochemical performance of NMC prepared by this method.

3. CONCLUSIONS

New insights into the all-dry synthesis of NMC622 cathode materials from RS-precursors were provided in this study. At temperatures below 723 °C (the melting point of Li_2CO_3), the kinetics of RS-precursor thermal lithiation to form NMC are slower than the thermal lithiation of HP-precursors. This has

https://doi.org/10.1021/acsomega.3c08702
ACS Omega 2024, 9, 1916–1924

many consequences. Because Li_2CO_3 remains unreacted at high temperature (>700 °C), a higher amount of excess Li is needed during NMC synthesis from RS-precursors to compensate for lithium loss from evaporation and to improve the compositional homogeneity of the final NMC. Despite the increased lithium excess required, increasing Li_2CO_3 costs, the elimination of wastewater production, and reduction in processing steps still make the all-dry synthesis route attractive compared to the coprecipitation route. The slower lithiation kinetics of RS-precursors also result in Li_2CO_3 being present in the liquid form during the lithiation reaction. The liquid Li_2CO_3 acts as a flux, resulting in simultaneously improvement of crystallinity and rapid RS-precursor lithiation and NMC primary particle growth at temperatures above the melting point of Li_2CO_3. As a result, the RS-precursor achieves its full lithiation extent at a lower temperature than that of the HP-precursor and a larger final primary particle size, even though its initial lithiation kinetics are slower. While the NMC made from the RS-precursor with 20% excess Li showed relatively similar ICE, polarization, and capacity retention compared to the NMC made from HP-precursor, its capacity was lower. This was attributed to compositional inhomogeneities in the RS-precursor. Future efforts are required to improve compositional homogeneity and lithiation kinetics for this all-dry synthesis route to provide a higher capacity NMC.

4. EXPERIMENTAL SECTION

4.1. Materials. NiO powder (Sigma-Aldrich, −325 mesh, 99%), MnO powder (Aldrich, −60 mesh, 99%), CoO powder (Alfa Aesar, 99.7%), Li_2CO_3 powder (Alfa Aesar, 99%), and commercial HP powder, $Ni_{0.6}Mn_{0.2}Co_{0.2}(OH)_2$ (Zoomwe), provided by CNGR Advanced Material Co., LTD, were used to synthesize the RS-precursor and NMC622 cathode materials in this study.

4.2. Sample Preparation. The RS-phase $[Ni_{0.6}Mn_{0.2}Co_{0.2}]O$ precursor was prepared by first combining stoichiometric amounts of NiO, MnO, and CoO (~20 g in total) with an automatic grinder (Retsch RM200 mortar grinder equipped with an agate mortar and pestle) for 3 h. The resulting mixture after grinding was then placed in an alumina crucible and heated in a tube furnace for 12 h at 1000 °C under an argon flow. An alumina crucible filled with MnO powder was placed upstream of the sample as an oxygen getter. The resulting RS-precursor was ground by hand in a mortar and pestle and then passed through a 53 μm sieve.

NMC622 cathode materials were prepared by hand-grinding either synthesized RS-precursor or commercial HPs, with Li_2CO_3 in a mortar and pestle until a homogeneous mixture was obtained (~10 min). To evaluate the effect of the excess Li content on the electrochemical performance of the NMC made from the RS-precursor, two different amounts of Li_2CO_3, corresponding to a 5 and 20% stoichiometric excess of lithium, were chosen, while a Li/TM ratio of 1.05 was used to make NMC from commercial HP. Each mixture was placed in an alumina crucible and heated in a tube furnace in air at 900 °C for 12 h. Finally, all the products were ground to fine powder by hand with mortar and pestle and passed through a 38 μm sieve (400-mesh). The resulting NMC samples are referred to here as NMC-RS-L5, NMC-RS-L20, and NMC-HP-L5 where L# denotes the percent excess lithium used, and RS and HP specify type of precursor from which the NMC was made.

4.3. Structural and Morphological Characterization. Powder X-ray diffraction (XRD) patterns were measured with a Rigaku Ultima IV X-ray diffractometer equipped with a Cu anode X-ray tube, a diffracted beam graphite monochromator, and a scintillation detector. The XRD patterns of the NMCs were also analyzed using the Rietveld refinement method, which is described in detail in Supporting Information Section S.A1. In addition, the degree of inhomogeneity (*i.e.*, standard deviations in Mn distribution, σ_x and σ_y) in the RS-precursor (σ_x) and NMCs (σ_y) were also calculated by modified Williamson−Hall (W−H) analysis, as reported in our previous study.[26] *In situ* XRD measurements of precursor samples during thermal lithiation were performed at the Canadian Light Source (CLS, Saskatoon, Saskatchewan, Canada) Brockhouse Diffraction Sector (BXDS) beamline. Further details of this experiment and associated data analysis methods are described in detail in Supporting Information Section S.A2.

Scanning electron microscopy (SEM) images were obtained using a JEOL JSM-IT200LA SEM. Energy-dispersive X-ray spectroscopy (EDS) elemental mapping images of the samples were also obtained by using a MIRA-3 TESCAN field emission scanning electron microscope (FESEM).

4.4. Electrochemical Analysis. Electrode slurry preparation was conducted by mixing active materials, carbon black (Super C65, Imerys Graphite and Carbon), and PVDF binder (polyvinylidene fluoride, Kynar HSV 900) with a mass ratio of 92/4/4 in an appropriate amount of *N*-methyl-2-pyrrolidone (Sigma-Aldrich, anhydrous 99.5%). Slurries were mixed for 15 min using a high shear mixer (1 in. diameter Cowles blade/5000 rpm) and then coated onto aluminum foil using a coating bar with a 0.015 cm gap and dried in air at 120 °C for 90 min. Electrode discs with loadings of ~1−1.1 mA h/cm^2 and 1.27 cm in diameter were punched from the as-prepared coatings and further heated under vacuum at 120 °C overnight before cell assembly. Coin cells (2325-type) were assembled with lithium foils (99.9%, Sigma-Aldrich) as counter/reference electrodes and two Celgard 2300 and one polypropylene blown microfiber nonwoven fabric (3M Company) separators. The electrolyte was 1 M $LiPF_6$ (BASF) in a solution of ethylene carbonate, diethylcarbonate, and monofluoroethylene carbonate (volume ratio 3:6:1, all from BASF). Cells were cycled between 2.5 and 4.3 V *vs* Li/Li$^+$ at 30.0 ± 0.1 °C with a Maccor Series 4000 Automated Test System. Cycling rates were calculated by assuming a capacity of 200 mA h/g. For constant current cycling, the first cycle was conducted at a rate of C/20 with a constant potential hold at 4.3 V until the current dropped to C/40 (to simulate constant current, constant voltage cycling in full cells). Subsequent cycles were conducted at a rate of C/5 with a constant potential hold at 4.3 V until the current dropped to C/10.

■ ASSOCIATED CONTENT

Supporting Information

The Supporting Information is available free of charge at https://pubs.acs.org/doi/10.1021/acsomega.3c08702.

Additional experimental details, materials, and methods, including photographs of *in situ* XRD analysis setup; SEM images of the mixture of the individual oxide precursors after grinding and the synthesized RS-precursor; integrated areas *vs* temperature plots; expanded views of the NMC(003) XRD peaks; summarized XRD refinement; and electrochemical performance results for the synthesized NMCs in this study (PDF)

https://doi.org/10.1021/acsomega.3c08702
ACS Omega 2024, 9, 1916−1924

AUTHOR INFORMATION

Corresponding Author

Mark N. Obrovac − *Department of Chemistry, Dalhousie University, Halifax, Nova Scotia B3H 4R2, Canada; Department of Physics and Atmospheric Science and Clean Technologies Research Institute, Dalhousie University, Halifax, Nova Scotia B3H 4R2, Canada;* orcid.org/0000-0001-5509-3185; Email: mnobrovac@dal.ca

Author

Mohammad H. Tahmasebi − *Department of Chemistry, Dalhousie University, Halifax, Nova Scotia B3H 4R2, Canada;* orcid.org/0000-0003-1907-5806

Complete contact information is available at: https://pubs.acs.org/10.1021/acsomega.3c08702

Notes

The authors declare no competing financial interest.

ACKNOWLEDGMENTS

The authors acknowledge funding from NSERC and NOVONIX Battery Testing Services under the auspices of the NSERC Alliance grants program (grant number ALLRP 558364-20). The authors would like to thank BXDS beamline scientist Adam Leontowich for his extensive support for carrying out *in situ* XRD experiments at CLS. M.H.T. appreciates the support of the Mitacs Accelerate Fellowship.

REFERENCES

(1) Zheng, J.; Kan, W. H.; Manthiram, A. Role of Mn Content on the Electrochemical Properties of Nickel-Rich Layered LiNi0.8−xCo0.1Mn0.1+xO2 ($0.0 \leq x \leq 0.08$) Cathodes for Lithium-Ion Batteries. *ACS Appl. Mater. Interfaces* **2015**, *7*, 6926−6934.

(2) Dixit, M.; Kosa, M.; Lavi, O. S.; Markovsky, B.; Aurbach, D.; Major, D. T. Thermodynamic and kinetic studies of LiNi 0.5 Co 0.2 Mn 0.3 O 2 as a positive electrode material for Li-ion batteries using first principles. *Phys. Chem. Chem. Phys.* **2016**, *18*, 6799−6812.

(3) Li, J.; Shunmugasundaram, R.; Doig, R.; Dahn, J. R. In Situ X-ray Diffraction Study of Layered Li-Ni-Mn-Co Oxides: Effect of Particle Size and Structural Stability of Core-Shell Materials. *Chem. Mater.* **2016**, *28*, 162−171.

(4) Wang, L.; Wu, B.; Mu, D.; Liu, X.; Peng, Y.; Xu, H.; Liu, Q.; Gai, L.; Wu, F. Single-crystal LiNi0.6Co0.2Mn0.2O2 as high performance cathode materials for Li-ion batteries. *J. Alloys Compd.* **2016**, *674*, 360−367.

(5) Li, J.; Cameron, A. R.; Li, H.; Glazier, S.; Xiong, D.; Chatzidakis, M.; Allen, J.; Botton, G. A.; Dahn, J. R. Comparison of Single Crystal and Polycrystalline LiNi0.5Mn0.3Co0.2O2 Positive Electrode Materials for High Voltage Li-Ion Cells. *J. Electrochem. Soc.* **2017**, *164*, A1534−A1544.

(6) Li, J.; Li, H.; Stone, W.; Weber, R.; Hy, S.; Dahn, J. R. Synthesis of Single Crystal LiNi0.5Mn0.3Co0.2O2 for Lithium Ion Batteries. *J. Electrochem. Soc.* **2017**, *164*, A3529−A3537.

(7) Li, H.; Li, J.; Ma, X.; Dahn, J. R. Synthesis of Single Crystal LiNi0.6Mn0.2Co0.2O2 with Enhanced Electrochemical Performance for Lithium Ion Batteries. *J. Electrochem. Soc.* **2018**, *165*, A1038−A1045.

(8) Huang, B.; Wang, M.; Zuo, Y.; Zhao, Z.; Zhang, X.; Gu, Y. The effects of reheating process on the electrochemical properties of single crystal LiNi0.6Mn0.2Co0.2O2. *Solid State Ionics* **2020**, *345*, 115200.

(9) Langdon, J.; Manthiram, A. A perspective on single-crystal layered oxide cathodes for lithium-ion batteries. *Energy Storage Mater.* **2021**, *37*, 143−160.

(10) Obrovac, M. N.; Zheng, L.; Garayt, M. D. L. Engineered Particle Synthesis by Dry Particle Microgranulation. *Cell Rep. Phys. Sci.* **2020**, *1*, 100063.

(11) Zheng, L.; Bennett, J. C.; Obrovac, M. N. All-Dry Synthesis of Single Crystal NMC Cathode Materials for Li-Ion Batteries. *J. Electrochem. Soc.* **2020**, *167*, 130536.

(12) Shi, Y.; Zhang, M.; Fang, C.; Meng, Y. S. Urea-based hydrothermal synthesis of LiNi0.5Co0.2Mn0.3O2 cathode material for Li-ion battery. *J. Power Sources* **2018**, *394*, 114−121.

(13) Nam, K.-M.; Kim, H.-J.; Kang, D.-H.; Kim, Y.-S.; Song, S.-W. Ammonia-free coprecipitation synthesis of a Ni-Co-Mn hydroxide precursor for high-performance battery cathode materials. *Green Chem.* **2015**, *17*, 1127−1135.

(14) Dong, H.; Koenig, G. M. A review on synthesis and engineering of crystal precursors produced via coprecipitation for multicomponent lithium-ion battery cathode materials. *CrystEngComm* **2020**, *22*, 1514−1530.

(15) Wagner, N. P.; Tolchard, J. R.; Tron, A.; Pollen, H. N.; Gaertner, H.; Vullum, P. E. Improved cyclability of Nickel-rich layered oxides. *MRS Adv.* **2020**, *5*, 1433−1440.

(16) Kim, Y. Lithium Nickel Cobalt Manganese Oxide Synthesized Using Alkali Chloride Flux: Morphology and Performance As a Cathode Material for Lithium Ion Batteries. *ACS Appl. Mater. Interfaces* **2012**, *4*, 2329−2333.

(17) Kimijima, T.; Zettsu, N.; Teshima, K. Growth Manner of Octahedral-Shaped Li(Ni1/3Co1/3Mn1/3)O2 Single Crystals in Molten Na2SO4. *Cryst. Growth Des.* **2016**, *16*, 2618−2623.

(18) Gupta, S. K.; Mao, Y. A review on molten salt synthesis of metal oxide nanomaterials: Status, opportunity, and challenge. *Prog. Mater. Sci.* **2021**, *117*, 100734.

(19) Qin, Z.; Wen, Z.; Xu, Y.; Zheng, Z.; Bai, M.; Zhang, N.; Jia, C.; Wu, H. B.; Chen, G. A Ternary Molten Salt Approach for Direct Regeneration of LiNi0.5Co0.2Mn0.3O2 Cathode. *Small* **2022**, *18*, 2106719.

(20) Azhari, L.; Meng, Z.; Yang, Z.; Gao, G.; Han, Y.; Wang, Y. Underlying limitations behind impedance rise and capacity fade of single crystalline Ni-rich cathodes synthesized via a molten-salt route. *J. Power Sources* **2022**, *545*, 231963.

(21) Qin, Z.; Zhang, T.; Gao, X.; Luo, W.; Han, J.; Lu, B.; Zhou, J.; Chen, G. Self-Reconstruction of Highly Degraded Li-$Ni_{0.8}Co_{0.1}Mn_{0.1}O_2$ toward Stable Single-Crystalline Cathode. *Adv. Mater.* **2023**, 2307091.

(22) Qin, Z.; Zhang, Y.; Luo, W.; Zhang, T.; Wang, T.; Ni, L.; Wang, H.; Zhang, N.; Liu, X.; Zhou, J.; Chen, G. A Universal Molten Salt Method for Direct Upcycling of Spent Ni-rich Cathode towards Single-crystalline Li-rich Cathode. *Angew. Chem., Int. Ed.* **2023**, *62*, No. e202218672.

(23) Ruess, R.; Ulherr, M. A.; Trevisanello, E.; Schröder, S.; Henss, A.; Janek, J. Transition Metal Oxides and Li2CO3 as Precursors for the Synthesis of Ni-Rich Single-Crystalline NCM for Sustainable Lithium-Ion Battery Production. *J. Electrochem. Soc.* **2022**, *169*, 070531.

(24) Tahmasebi, M. H.; Zheng, L.; Hatchard, T. D.; Obrovac, M. N. Li[Ni0.6Mn0.2Co0.2]O2Made From Crystalline Rock Salt Oxide Precursors. *J. Electrochem. Soc.* **2023**, *170*, 030531.

(25) Garayt, M. D. L.; Zhang, N.; Yu, S.; Abraham, J. J.; Murphy, A.; Omessi, R.; Ye, Z.; Azam, S.; Johnson, M. B.; Yang, C.; Dahn, J. R. Single Crystal Li1+x[Ni0.6Mn0.4]1-xO2Made by All-Dry Synthesis. *J. Electrochem. Soc.* **2023**, *170*, 060529.

(26) Tahmasebi, M. H.; Obrovac, M. N. Quantitative Measurement of Compositional Inhomogeneity in NMC Cathodes by X-ray Diffraction. *J. Electrochem. Soc.* **2023**, *170*, 080519.

(27) Wu, F.; Tian, J.; Su, Y.; Wang, J.; Zhang, C.; Bao, L.; He, T.; Li, J.; Chen, S. Effect of Ni2+ Content on Lithium/Nickel Disorder for Ni-Rich Cathode Materials. *ACS Appl. Mater. Interfaces* **2015**, *7*, 7702−7708.

(28) Rathore, D.; Liang, C.; Zsoldos, E.; Ball, M.; Yu, S.; Yang, C.; Wang, Q.; Dahn, J. R. Elucidating the Role of Excess Li in the Electrochemical Performance of Li1+x[Ni0.5Mn0.5]1-xO2 Layered Oxides. *J. Electrochem. Soc.* **2023**, *170*, 020520.

(29) Weber, R.; Li, H.; Chen, W.; Kim, C.-Y.; Plucknett, K.; Dahn, J. R. In Situ XRD Studies During Synthesis of Single-Crystal LiNiO2,

LiNi0.975Mg0.025O2, and LiNi0.95Al0.05O2 Cathode Materials. *J. Electrochem. Soc.* **2020**, *167*, 100501.

https://doi.org/10.1021/acsomega.3c08702
ACS Omega 2024, 9, 1916−1924